C. R. Chimie 18 (2015) 178–186

Contents lists available at ScienceDirect

Comptes Rendus Chimie

www.sciencedirect.com

Full paper/Mémoire

Study of a Mn–Cr/TiO_2 mixed oxide nanocatalyst prepared via an inorganic precursor complex for high-temperature water–gas shift reaction

Javad Farzanfar, Ali Reza Rezvani *

Department of Chemistry, University of Sistan and Baluchestan, PO Box 98135-674, Zahedan, Iran

ARTICLE INFO

Article history:
Received 22 January 2014
Accepted after revision 20 May 2014
Available online 31 December 2014

Keywords:
Novel precursor
$[Mn(H_2O)_6]_3[Cr(NCS)_6]_2{\cdot}H_2O/TiO_2$
Complex
Bimetallic nanocatalyst
High-temperature water–gas shift reaction

ABSTRACT

The influence of three preparation methods on the properties and reaction performances of a titania-supported Mn–Cr bimetallic nanocatalyst for high-temperature water–gas shift reaction has been studied. Impregnation, co-precipitation and thermal decomposition of the $[Mn(H_2O)_6]_3[Cr(NCS)_6]_2{\cdot}H_2O/TiO_2$ precursor as an inorganic precursor complex were utilized for the preparation of the Mn–Cr/TiO_2 catalysts. The calcined catalyst and the precursor that were used for its preparation were characterized by powder X-ray diffraction, scanning electron microscopy, Brunauer–Emmett–Teller specific surface area measurements, thermal gravimetric analysis, differential scanning calorimetry and Fourier transform–infrared spectroscopy. The high-temperature water–gas shift activity was appraised in the temperature range from 280 to 420 °C. The results showed that thermal decomposition of inorganic precursor complexes is more advantageous than impregnation and co-precipitation methods for the preparation of Mn–Cr/TiO_2 catalysts for high-temperature water–gas shift reaction.

© 2014 Académie des sciences. Published by Elsevier Masson SAS. All rights reserved.

1. Introduction

The solid-catalyzed water–gas shift (WGS) reaction, ($CO + H_2O \rightleftharpoons CO_2 + H_2$), in which carbon monoxide and water are transformed into hydrogen and carbon dioxide is one of the most significant steps in several industrial processes [1–3]. Solid catalysts have been widely applied to industrial catalytic processes in order to produce pure hydrogen, and diminish CO in H_2-rich reformates, or to control the H_2/CO ratio in syngas [4–6]. Recently, WGS reaction is expanded in fuel-cell technology since it is appropriate for removing a high percentage of CO by controlling reaction temperatures [6–11].

As a result of the moderate exothermicity (ΔH_{298} = –41.1 kJ mol^{-1}), the WGS reaction is carried out in two separate stages, employing catalysts that have been particularly designed for each stage. The first step includes a high-temperature conversion (300–400 °C) employing an iron–chromium spinel catalyst, and the second step involves a lower temperature process (200–250 °C) with a highly active copper–zinc oxide catalyst [12–14]. A promoted manganese oxide catalyst has been also investigated to ascertain its suitability for the WGS reaction.

In earlier studies, manganese and chromium oxide catalysts were prepared by co-precipitation [14,15], sol–gel (organic acid complex) [16–18] and combustion [19–22] methods for various catalytic processes. The object of this work is the investigation of the influences of the preparation method on the structure and performance of Mn–Cr/TiO_2 catalysts for WGS reaction. We also report supplemental results regarding the Mn–Cr/TiO_2

* Corresponding author.
E-mail addresses: Ali@hamoon.usb.ac.ir (J. Farzanfar), javadfr@pgs.usb.ac.ir (A.R. Rezvani).

http://dx.doi.org/10.1016/j.crci.2014.05.007
1631-0748/© 2014 Académie des sciences. Published by Elsevier Masson SAS. All rights reserved.

catalyst that was prepared via thermal decomposition of titania-supported $[Mn(H_2O)_6]_3[Cr(NCS)_6]_2{\cdot}H_2O$ as a supported inorganic complex precursor. A comparative analysis of the physicochemical features was performed by using X-ray diffraction (XRD), scanning electron microscopy (SEM), Brunauer–Emmet–Teller (BET) surface area measurement, thermal gravimetric analysis (TGA) and differential scanning calorimetry (DSC).

The use of inorganic precursor complexes as a novel approach for the preparation of materials, including two (or more) metallic ions or oxide phases can provide many benefits, such as excessive metal interactions, homogeneous dispersion of the two (or more) metallic ions in the entire part of the support and maximum loading amount, which promote catalytic performance [23–28].

2. Experimental

2.1. Materials

Reagent-grade $Cr(NO_3)_3{\cdot}9H_2O$, $Mn(NO_3)_2{\cdot}4H_2O$ and NH_4SCN (ammonium thiocyanate) were purchased from Aldrich and used as received. Bare titanium dioxide with a specific surface area of 82 m^2/g was used as received as a catalytic support.

2.2. Preparation of the catalysts

2.2.1. Preparation of $[Mn(H_2O)_6]_3[Cr(NCS)_6]_2{\cdot}H_2O$

Ammonium thiocyanate (913 mg, 12 mmol) was dissolved in water (5 mL), and was added drop wise, under continuous stirring, to an aqueous solution (10 mL) of $Cr(NO_3)_3{\cdot}9H_2O$ (800 mg, 2 mmol). After 6 h of stirring at room temperature, $Mn(NO_3)_2{\cdot}4H_2O$ (753 mg, 3 mmol) was added to the present solution. The reaction mixture was stirred during 4 h and then left to stand at room temperature in the air. After two weeks, water-dissoluble and lavender crystals were achieved in ca. 68%. Anal. calc. for $C_{12}H_{38}Cr_2Mn_3N_{12}O_{19}S_{12}$ (1308.09 g): C, 11.02; H, 2.93; N, 12.85. Found: C, 10.87; H, 2.88; N, 12.81%. IR (KBr, cm^{-1}): 3436, 3159, 2098, 1618, 825, 480. UV–vis (H_2O, nm): 212, 269, 313, 409, 565.

2.2.2. Preparation of $[Mn(H_2O)_6]_3[Cr(NCS)_6]_2{\cdot}H_2O/TiO_2$ precursor

Calculated amounts of $[Mn(H_2O)_6]_3[Cr(NCS)_6]_2{\cdot}H_2O$ (10 mmol, 13,080 mg) were dissolved in 100 mL of distilled water and then TiO_2 (600 mg) was added to this solution. The achieved suspension was stirred and vaporized at 30 °C to dehydration.

2.2.3. Preparation of titania-supported manganese–chromium catalyst, Mn–Cr/TiO_2

In order to gain the final calcined 60%Mn/40%Cr on molar basis/5 wt%TiO_2 catalyst, the $[Mn(H_2O)_6]_3[Cr(NCS)_6]_2{\cdot}H_2O/TiO_2$ precursor was calcined at 600 °C for 4 h under a static air atmosphere in an electric furnace. The final obtained grey Mn–Cr/TiO_2 catalyst (atomic %: 14.3%Mn/10.1%Cr) was generated and retained in desiccator. This sample is labelled as MnCrTiIPC (thermal decomposition of inorganic precursor complex method).

2.2.4. Preparation of reference catalysts

For the sake of comparison, the Mn–Cr/TiO_2 reference catalysts were obtained through impregnation and co-precipitation procedures. The co-precipitation method consists of mixing aqueous solutions of chromium nitrate ($Cr(NO_3)_3{\cdot}9H_2O$) and manganese nitrate ($Mn(NO_3)_2{\cdot}4H_2O$) (2:3) with the required quantity of titania and Na_2CO_3 at 30 °C, keeping a constant pH value through pouring drop wise an aqueous solution of NaOH and aging the resulting precipitate for 6 h. After aging, the suspension was filtered and washed. Subsequently, the precipitate was dried at 120 °C and finally calcined at 600 °C for 4 h (atomic %: 14.6%Mn/9.7%Cr). In the impregnation method, calculated amounts of chromium nitrate and manganese nitrate were dissolved in water and impregnated onto the titania support. The suspension, after having been aged for 6 h at 30 °C, was then filtered, followed by drying overnight at 120 °C; in order to attain the final calcined catalyst, the precursor was then calcined at 600 °C for 4 h (atomic %: 14.3%Mn/9.5%Cr). These samples are labelled as MnCrTiCP (co-precipitation method) or MnCrTiIM (impregnation method), respectively.

2.3. Catalyst characterization

2.3.1. X-ray diffraction (XRD)

Powder XRD measurements were performed using a FK60-04 diffractometer. Scans were taken with a 2θ step size of 0.02° using a Cu Kα radiation source. Data were collected over a 2θ range from 5 to 90° and phases were identified by matching the experimental patterns to the PDF database provided via the International Center for Diffraction Data (PDF2-Diffraction Database File).

2.3.2. Thermal gravimetric analysis (TGA)

The weight changes in the catalyst precursor were measured by using TGA-PL England equipment under a flow of dry air. The temperature was raised from room temperature up to 600 °C using a linear programmer at a heating rate of 10 °C per min. The sample weight was between 15 and 20 mg.

2.3.3. Differential scanning calorimetry (DSC)

DSC was carried out on a Netzsch DSC 200 F3 equipment under a flow of dry air, using a linear programmer at heating rate of 10 °C per min.

2.3.4. Scanning electron microscopy (SEM)

The morphology of the catalysts and their precursors were observed using a Jeol JSM 5410 scanning electron microscope instrument operating at 10 kV.

2.3.5. Brunauer–Emmett–Teller (BET) surface area measurements

The BET surface areas and pore volumes of the precursor and calcined catalysts were measured using N_2 physisorption by means of a Quantachrome Nova 4200 apparatus. Each sample was degassed under nitrogen atmosphere at 300 °C for 3 h. In order to obtain the BET surface areas and pore volumes, different samples were evacuated at −196 °C for 66 min.

2.3.6. Elemental analysis, FT–IR, UV–Vis and atomic absorption spectroscopy

Elemental analysis was carried out using a Perkin-Elmer 2400 CHNS/O elemental analyzer. FT–IR spectra were recorded as KBr pellets on a FT–IR JASCO 460 spectrophotometer. UV–Vis spectra were obtained on a JASCO 7850 spectrophotometer. Atomic absorption spectroscopy on metals was performed via Varian AA50 equipment.

2.4. Catalytic activity tests

WGS activity tests were carried out in a fixed bed micro-reactor at the atmospheric pressure. Before catalytic runs, the catalysts (1000 mg; $50 < d < 100$ μm; without further sieving, dilution or purification) were subjected to a reduction in situ at the atmospheric pressure under a flowing H_2–N_2 stream ($N_2/H_2 = 1$, flow rate of each gas = 30 mL·min^{-1}) at 400 °C for 6 h. Subsequently, a H_2O/CO mixture (the composition of the reaction mixture: 4/1) with a GHSV of 3600 h^{-1} was used instead of the N_2/H_2 one. WGS activity tests were performed between 280 and 420 °C, 8 h for each temperature. The analysis of the reactor inlet and outlet gases was carried out on line by means of a gas chromatograph (Varian, Model 3400 series). CO conversion and CO_2 selectivity were used for evaluation of catalyst activity:

(I) CO conversion (%) = {[(moles of CO_{in}) – (moles of CO_{out})]/moles of CO_{in}} × 100

(II) CO_2 selectivity (%) = [moles of CO_2/moles of products] × 100

3. Results and discussion

3.1. Complex characterization

3.1.1. Structure description

The reaction of the molecular ion, $[Cr(NCS)_6]^{3-}$ with the complementary unit $[Mn(H_2O)_6]^{2+}$ at room temperature (298 K) led to the formation of the bimetallic complex. The details of the successive reactions are condensed in Eqs. (1) and (2).

$$2\,Cr(NO_3)_3{\cdot}9H_2O + 12\,NH_4NCS \rightarrow 2\,(NH_4)_3[Cr(NCS)_6] + 6\,NH_4NO_3 + 6\,H_2O \quad (1)$$

$$2\,(NH_4)_3[Cr(NCS)_6] + 3\,[Mn(H_2O)_6](NO_3)_2 \rightarrow [Mn(H_2O)_6]_3[Cr(NCS)_6]_2 + 6\,NH_4NO_3 \quad (2)$$

3.1.2. Infrared spectroscopy

The infrared spectrum of the $[Mn(H_2O)_6]_3[Cr(NCS)_6]_2{\cdot}H_2O$ complex (Fig. 1) shows two sets of vibrations due to the thiocyanate and aqua ligands. The $\nu(H_2O)$ vibrations correlated with both coordination types, and free water molecules are perceived as very strong and broad bands in the 3600–3430 and 3250–3100 cm^{-1} regions, respectively. The sharp band at 1618 cm^{-1} is also ascribed to the crystallization of water molecules in the crystal lattice [29]. The ν(C–N) stretching vibration in the thiocyanate ligand is observed for the desired complex as an intensive band at 2098 cm^{-1}. The absorption band at 480 cm^{-1} is from the δ(N–C–S) bending mode in the thiocyanate ligand. Moreover, the ν(C=S) stretching mode emerges in the spectrum of the free thiocyanate ligand as a sharp band at 749 cm^{-1}, whereas, in the desired complex, this band is shifted to 825 cm^{-1}. These characteristic IR bands, related to the vibrations of the thiocyanate groups, corroborate the nitrogen-bonding mode of the thiocyanate ligands to the chromium ion [30,31].

3.1.3. Atomic absorption and electronic spectroscopy

The atomic absorption spectroscopy analysis of the desired complex gives adequate values for Cr(III) and Mn(II) ions, consequently revealing the presence of those metals.

The electronic excitation study of $[Mn(H_2O)_6]_3[Cr(NCS)_6]_2{\cdot}H_2O$ complex in water solution displays several absorption bands in the UV and visible regions (Fig. 2). In the visible region, the broad absorption bands at 409 and 565 nm were ascribed to *d*–*d* transitions

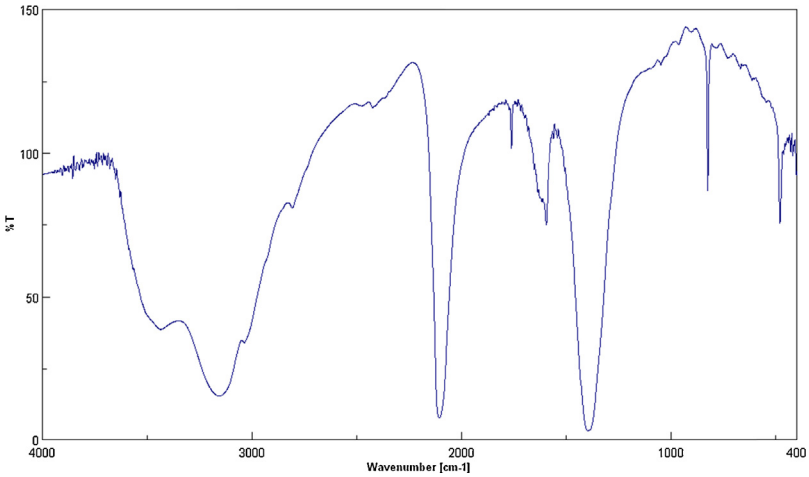

Fig. 1. FT–IR spectrum of $[Mn(H_2O)_6]_3[Cr(NCS)_6]_2{\cdot}H_2O$.

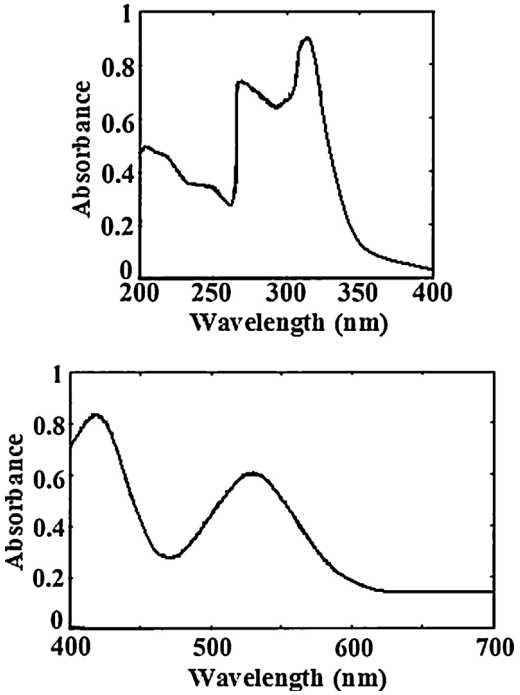

Fig. 2. Electronic spectra of $[Mn(H_2O)_6]_3[Cr(NCS)_6]_2{\cdot}H_2O$.

$^4A_{2g} \rightarrow {}^4T_{2g}$, $^4A_{2g} \rightarrow {}^4T_{1g}$ (F) in octahedral Cr(III) ion. In the UV region, two intense absorption bands at 212 and 269 nm were assigned to the intra-ligand $n \rightarrow \pi^*$ and $\pi \rightarrow \pi^*$ transitions of the thiocyanate ligand. The very intensive absorption band at 313 nm was attributed to ligand-to-metal charge transfer (LMCT).

3.2. Characterization of catalysts

3.2.1. X-ray diffraction

The XRD pattern for the precursor is shown in Fig. 3 and, as expected for a well-crystallized sample, the high intense and low half-width diffraction lines are perceived in the XRD pattern of the precursor (at $2\theta = 8.9$, 9.8, 10.7, 11.8, 12.7, 15.1, 17.8, 19.0, 23.3, 26.0, 26.7, and 27.5°). Fig. 4 exhibits the XRD pattern of the calcined MnCrTiIPC catalyst prepared from a novel precursor. Additionally, the XRD patterns of the both calcined MnCrTiIM and MnCrTiCP catalysts prepared by impregnation and co-precipitation are also presented as references in Fig. 4. All the samples display the characteristic diffraction peaks of Mn_2O_3 (JCPDS 41-1442), Cr_2O_3 (JCPDS 01-1294) and TiO_2 (JCPDS 04-0477). Only for calcined catalysts prepared from a novel precursor, three manganese–chromium mixed oxide phases, Mn_2CrO_4 (JCPDS 36-0546), $Mn_{1.5}Cr_{1.5}O_4$ (JCPDS 33-0892) and $CrMn_{1.5}O_4$ (JCPDS 44-0909) are observed. It could be deduced that in the calcined MnCrTiIPC catalyst, the amounts of three manganese–chromium mixed oxide phases are higher compared to Mn–Cr reference catalysts (MnCrTiIM and MnCrTiCP), and the thermal decomposition of inorganic precursor complex method promotes the chemical interactions between Mn–Cr–O species. The average sizes of these crystallites present on the calcined MnCrTiIPC catalyst and the calcined reference MnCrTiIM and MnCrTiCP catalysts were calculated by applying the Scherrer equation to Mn_2O_3 (222), Mn_3O_4 (311), Cr_2O_3 (116), Mn_2CrO_4 (311), $Mn_{1.5}Cr_{1.5}O_4$ (311) and $CrMn_{1.5}O_4$ (311) crystallographic planes (Table 1). The average particle sizes were smaller for the calcined MnCrTiIPC catalyst than those for reference Mn–Cr catalysts prepared by impregnation and co-precipitation methods. These results point out that the thermal decomposition of inorganic precursor complex method led to the promotion of the dispersion of the above-mentioned phases and facilitates the generation of particles smaller than those present on the MnCrTiIM and MnCrTiCP catalysts. The XRD analysis of the reduced Mn–Cr/TiO_2 catalyst (Fig. 5) revealed that the above-mentioned phases decomposed, leading to the existence of MnO_2 (JCPDS 42-1316) and Cr_2O_3 (JCPDS 01-1294) phases.

3.2.2. Thermal analysis

To evaluate the thermal stability of $[Mn(H_2O)_6]_3[Cr(NCS)_6]_2{\cdot}H_2O$ complexes, thermal gravimetric analysis

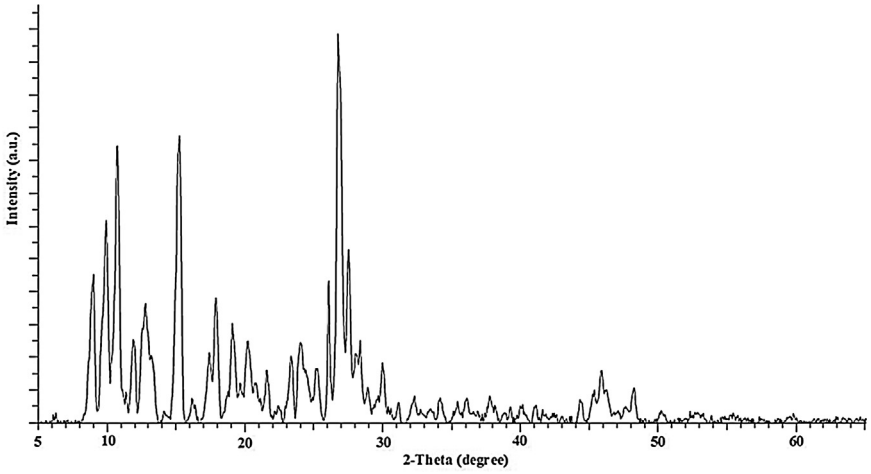

Fig. 3. Powder x-ray diffraction pattern of $[Mn(H_2O)_6]_3[Cr(NCS)_6]_2{\cdot}H_2O/TiO_2$ precursor.

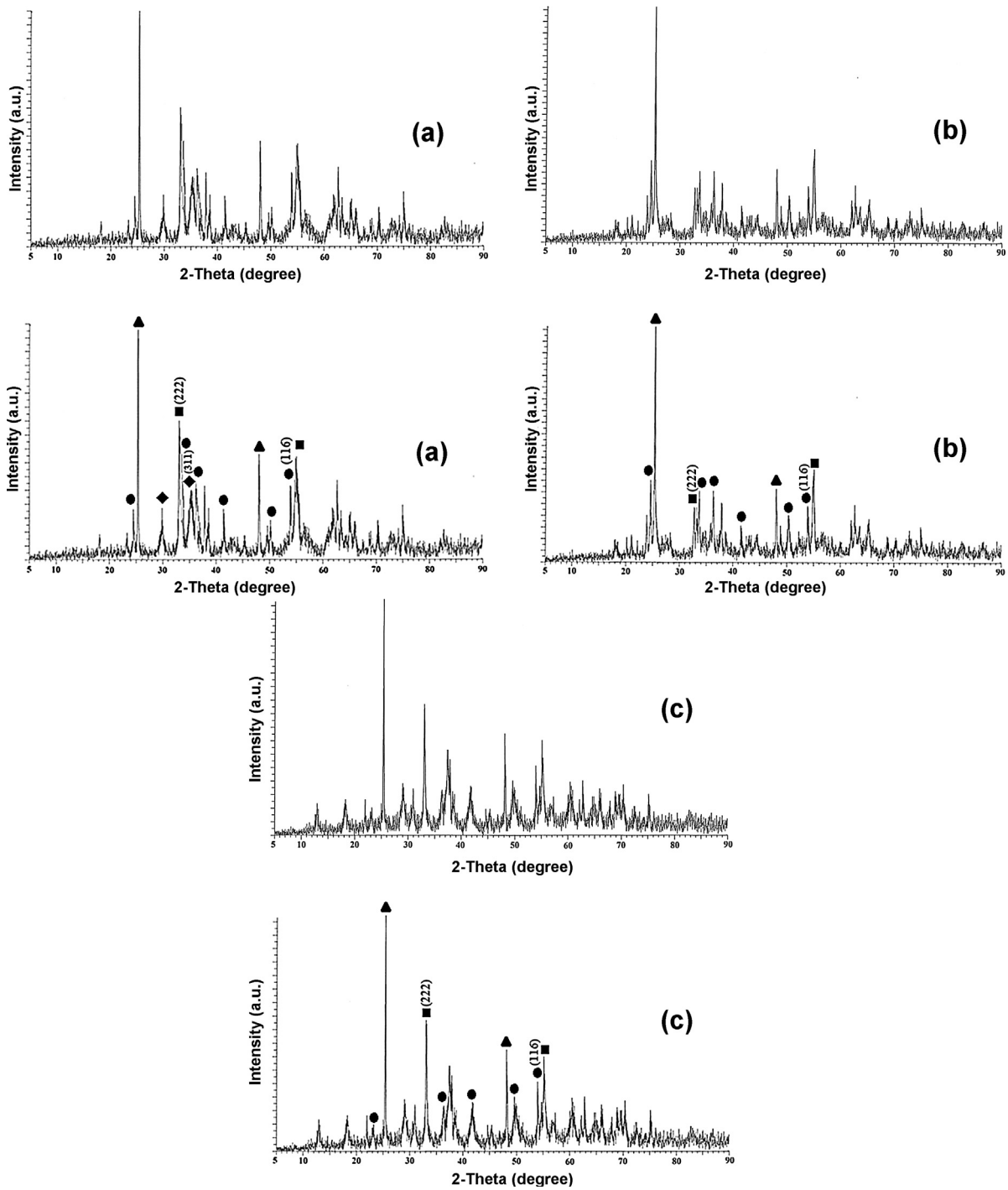

Fig. 4. Powder x-ray diffraction patterns of (a) calcined MnCrTiIPC catalyst and reference catalysts prepared by (b) impregnation, and (c) co-precipitation: ▲ – TiO_2 (JCPDS 04-0477); ■ – Mn_2O_3 (JCPDS 41-1442); ● – Cr_2O_3 (JCPDS 01-1294); ◆ – Mixed oxide phases.

(TGA) was carried out on $[Mn(H_2O)_6]_3[Cr(NCS)_6]_2{\cdot}H_2O/TiO_2$ precursor at a heating rate of 10 °C min^{-1} in the temperature range from 30 to 600 °C (Fig. 6). Three main thermal effects are observed in the TGA-DTG profile of this precursor. Upon increasing the temperature, the first and second degradation steps take place within the temperature range 80–230 °C (DTG_{max} peaks at 110.62 and 187.54 °C), and they are attributed to the elimination of lattice and coordinated water molecules, respectively. The dehydrated species are stable up to 240 °C and, upon further heating, indicate another step of weight loss, which continued up to 600 °C. This last step of weight change (DTG_{max} peaks at 249.81, 273.40 and 481.71 °C) is attributed to the decomposition of coordinated

Table 1
Structural parameters of Mn–Cr/TiO_2 catalysts.

Sample	*d* (Mn_2O_3, nm)	*d* (Cr_2O_3, nm)	*d* (mixed oxide phases, nm)
MnCrTiIPC catalyst	15.78	11.34	15.9
Reference MnCrTiCP catalyst	31.52	34.09	
Reference MnCrTiIM catalyst	31.53	34.07	

thiocyanate ligands. Therefore, the stable oxide phases, as characterized by X-ray diffraction measurements, are generated as the final decomposition products.

Differential scanning calorimetry (DSC) measurement provided additional data for the existence of the diverse components and appraises their thermal behavior. As shown for the $[Mn(H_2O)_6]_3[Cr(NCS)_6]_2{\cdot}H_2O/TiO_2$ precursor in Fig. 7, one endothermic peak within the temperature range between 80 and 130 °C represents the elimination of the water molecules from the catalyst precursor, while the two exothermic peaks in the temperature range of 220–320 °C are referred to the degradation of the thiocyanate ligands and the four exothermic peaks between 320 and 590 °C are associated with the generation of the stable oxide phases. This was confirmed by the characterization of the final decomposition products by X-ray diffraction analysis.

3.2.3. SEM findings

In order to comprehend the details of the morphological changes, the precursor and calcined catalyst (MnCrTiIPC) were characterized by scanning electron microscopy (SEM) and their SEM micrographs are shown in Fig. 8. The SEM results revealed that the precursor and calcined sample have different morphologies and textures. The SEM image of the catalyst precursor was found to be comprised of several agglomerates of crystalline shaped particles with dissimilar sizes (Fig. 8a). The calcination process at 600 °C for 4 h brings about changes in the structural features of the calcined catalyst. In the calcined MnCrTiIPC catalyst, the agglomerate sizes are smaller than those at the catalyst precursor (Fig. 8b).

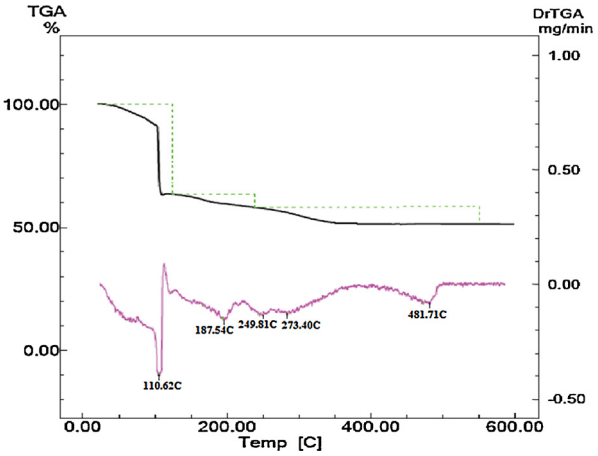

Fig. 6. Thermogram of $[Mn(H_2O)_6]_3[Cr(NCS)_6]_2{\cdot}H_2O/TiO_2$ precursor.

3.2.4. BET measurements

The surface areas of the catalyst precursor and of all calcined materials were measured by BET and the results are reported in Table 2. As shown, the catalyst precursor has lower BET specific surface area and pore volume (1.5 m^2/g and 0.1 cm^3/g, respectively) than the calcined MnCrTiIPC catalyst (141.9 m^2/g and 1.6 cm^3/g, respectively). The results also displayed that the calcined MnCrTiIPC catalyst has a higher BET specific surface area and pore volume than the calcined reference MnCrTiIM and MnCrTiCP catalysts. The usage of the suitable preparation method (thermal decomposition of $[Mn(H_2O)_6]_3[Cr(NCS)_6]_2{\cdot}H_2O/TiO_2$ precursor as inorganic precursor complex) led to an increment in the BET specific surface area and pore volume of the calcined MnCrTiIPC catalyst. All are adequate evidence for the enhancement of the dispersion of the active oxide phases and the improvement in catalytic performance of this calcined

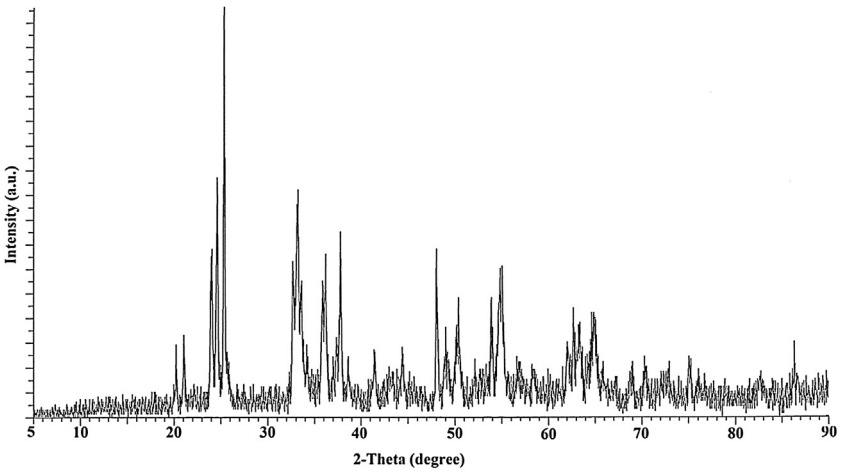

Fig. 5. Powder X-ray diffraction pattern of the reduced MnCrTiIPC catalyst.

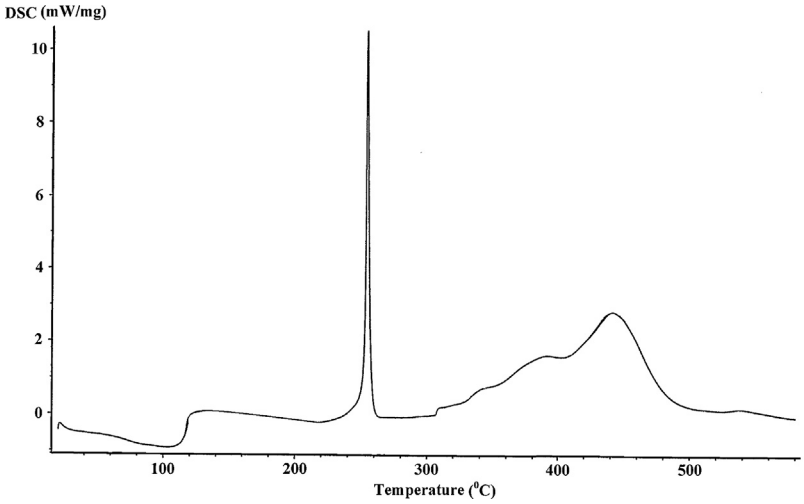

Fig. 7. DSC curve for the $[Mn(H_2O)_6]_3[Cr(NCS)_6]_2{\cdot}H_2O/TiO_2$ precursor.

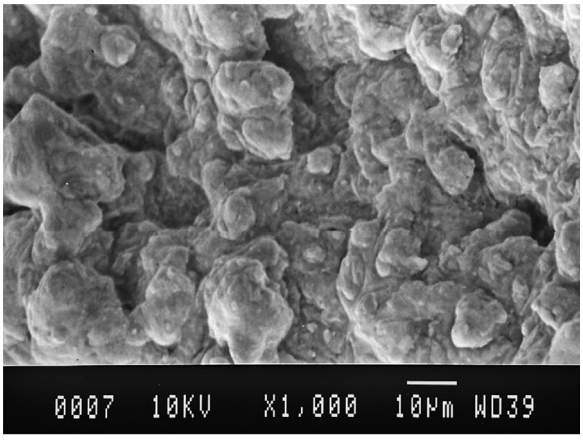

(a)

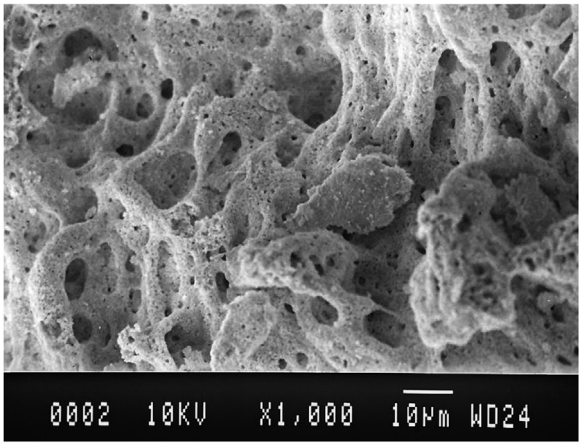

(b)

Fig. 8. SEM micrographs of: (a) $[Mn(H_2O)_6]_3[Cr(NCS)_6]_2{\cdot}H_2O/TiO_2$ precursor, and (b) calcined MnCrTiIPC catalyst.

MnCrTiIPC catalyst. The BET data of the catalyst precursor and all of calcined catalysts are in excellent coincidence with the SEM results; as expected, the finer particles for the calcined catalyst should has higher BET specific surface area and pore volume than the precursor.

3.3. WGSR activity measurements

3.3.1. Effect of temperature

The temperature dependence of CO conversion, CO_2 selectivity and methane selectivity over the calcined Mn–Cr/TiO_2 oxide catalysts prepared by impregnation, co-precipitation and thermal decomposition of inorganic precursor complex methods for high-temperature water–gas shift reaction in the temperature interval from 280 to 420 °C are illustrated in Fig. 9.

The WGSR activity of the calcined MnCrTiIPC catalyst increased with increasing temperature in the 280–320 °C interval and 72.6% CO conversion was achieved at 320 °C and, on the contrary, decreased with increasing temperature in the 320–420 °C interval and 61.3% CO conversion was achieved at 420 °C. In view of the temperate exothermicity of the water–gas shift reaction, according to Le Chatelier's principle, an increase in temperature decreases the CO conversion and CO_2 selectivity because, with increasing temperature in the WGS reaction, the equilibrium prefers the reverse reaction that may also lead to the formation of by-products (generation of methane by using methanation reaction, etc.) [32].

Table 2
Textural properties of the precursor and Mn–Cr/TiO_2 catalysts prepared using different methods.

Sample	BET surface area (m^2/g)	Pore volume (cm^3/g)
$[Mn(H_2O)_6]_3[Cr(NCS)_6]_2{\cdot}H_2O/TiO_2$	1.5	0.1
MnCrTiIPC catalyst	141.9	1.6
Reference MnCrTiCP catalyst	96.4	0.9
Reference MnCrTiIM catalyst	83.6	0.6

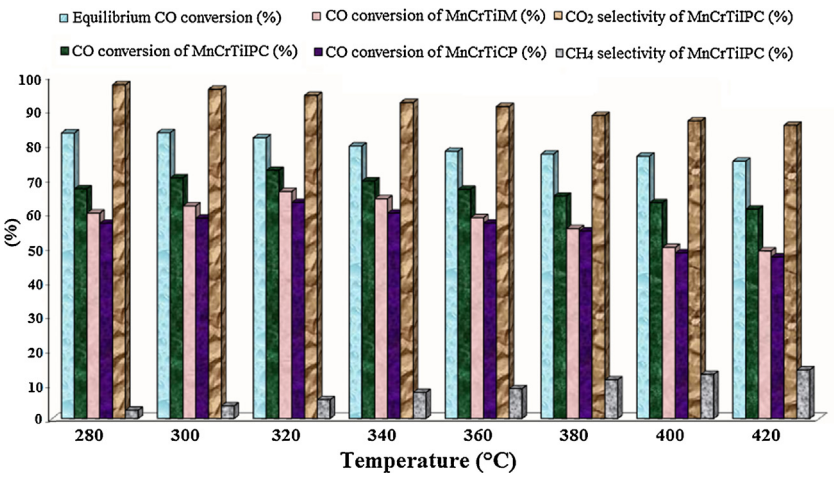

Fig. 9. (Color online.) Effect of reaction temperature on CO conversion, CO_2 selectivity and methane selectivity of MnCrTiIPC and reference Mn–Cr/TiO_2 catalysts in the water–gas shift reaction.

The MnCrTiIPC sample exhibited a considerably higher catalytic activity than those observed in the case of the reference MnCrTiIM and MnCrTiCP catalysts. The preparation method of the catalyst influences the catalytic activity and behavior of the catalyst. The decrement in the crystallite size, the increment in the BET specific surface area and the improvement in the catalytic performance of the calcined MnCrTiIPC catalyst in comparison with the findings achieved for the reference MnCrTiIM and MnCrTiCP catalysts become relevant to the exclusive features of the adopted preparation method. The inorganic precursor complexes method has a great advantage in the control of the size and bimetallic composition that it offers. Thus, most of the yielded nanoparticles would retain the original bimetallic composition of the inorganic precursor complex. This distinctly demonstrates the effectiveness of inorganic complexes as catalyst precursors.

3.3.2. Stability test

Another advantageous preference of the calcined MnCrTiIPC catalyst is its stability. The catalytic stability measurements were carried out over all of calcined catalysts at 320 °C, a temperature at which these catalysts achieved the maximum CO conversion. The profile of CO conversion versus time for these catalysts is illustrated in Fig. 10. The WGS activity of the whole calcined catalysts was almost stable within the 8-h test. The CO conversion of the calcined MnCrTiIPC catalyst decreases by 2.4% in the period of the 24-h test. After catalytic measurements, the morphological properties of the calcined Mn–Cr catalysts were changed; in other words, the tested catalysts are comprised of larger multiform particles compared with untested catalysts, which may be due to the occurrence of the sintering phenomena and adherence of small grains to the large particles. Therefore, it leads to a decrease in the catalytic activities.

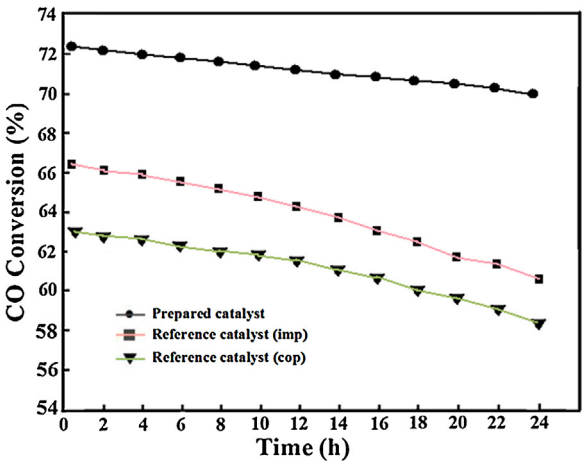

Fig. 10. Stability performances of Mn-Cr/TiO_2 catalysts prepared using different methods at 320 °CC.

4. Conclusions

The utilization of impregnation, co-precipitation and thermal decomposition of inorganic precursor complex methods provide Mn–Cr/TiO_2 oxide catalysts with different textural and morphological features. The analysis of the various properties of $[Mn(H_2O)_6]_3[Cr(NCS)_6]_2{\cdot}H_2O$ complex, precursor, and calcined catalyst by using different techniques, containing XRD, SEM, BET, TGA, DSC and FT–IR spectroscopy allowed us to verify that the calcination process results in the generation of solid chromium and manganese oxides as well as of gaseous carbon and nitrogen oxides.

The assessment of catalytic activity in high-temperature water–gas shift reaction showed that the thermal decomposition of $[Mn(H_2O)_6]_3[Cr(NCS)_6]_2{\cdot}H_2O/TiO_2$ precursor is a promising alternative route for the preparation of highly dispersed supported manganese–chromium oxide catalysts. Catalytic measurements in the temperature interval from 280 to 420 °C allowed us to certify the preferable performance of the MnCrTiIPC catalyst over the reference MnCrTiIM and MnCrTiCP catalysts. It is suggested that the higher activity of this sample is associated with the smaller particle sizes and higher BET specific

surface area compared with other manganese–chromium catalysts and other similar catalytic systems [15,22–24].

Acknowledgement

The authors are grateful to the USB for financial support.

References

[1] T. Baier, G. Kolb, Chem. Eng. Sci. 62 (2007) 4602.
[2] M. Laniecki, M. Ignacik, Catal. Today 116 (2006) 400.
[3] C. Ratnasamy, J. Wagner, Catal. Rev. 51 (2009) 325.
[4] Y. Li, Q. Fu, M.F. Stephanopoulos, Appl. Catal. B: Environ. 27 (2000) 179.
[5] F. Huber, J. Walmsley, H. Venvik, A. Holmen, Appl. Catal. A: Gen. 349 (2008) 46.
[6] Y. Tanaka, T. Takeguchi, R. Kikuchi, K. Eguchi, Appl. Catal. A: Gen. 279 (2005) 59.
[7] A. Boudjemaa, C. Daniel, C. Mirodatos, M. Trari, A. Auroux, R. Bouarab, C.R. Chimie 14 (2011) 534.
[8] C. Zerva, C.J. Philippopoulos, Appl. Catal. B: Environ. 67 (2006) 105.
[9] Y. Tanaka, T. Utaka, R. Kikuchi, T. Takeguchi, K. Sasaki, K. Eguchi, J. Catal. 215 (2003) 271.
[10] T. Utaka, K. Sekizawa, K. Eguchi, Appl. Catal. A: Gen. 194–195 (2000) 21.
[11] R. Bouarab, A. Boudjemaa, M. Trari, S. Bennici, A. Auroux, C.R. Chimie 12 (2009) 527.
[12] D. Mendes, S. SandraSá, J.M. Tosti, L.M. Sousa, A. Madeira, Mendes, Chem. Eng. Sci. 66 (2011) 2356.
[13] R. Kam, J. Scott, R. Amal, C. Selomulya, Chem. Eng. Sci. 65 (2010) 6461.
[14] G.J. Hutchings, R.G. Copperthwaite, F.M. Gottschalk, R. Hunter, J. Mellor, S.W. Orchard, T. Sangiorgio, J. Catal. 137 (1992) 408.
[15] F.M. Gottschalk, G.J. Hutchings, Appl. Catal. 51 (1989) 127.
[16] T. Fukunaga, N. Ryumon, N. Ichikuni, S. Shimazu, Catal. Commun. 10 (2009) 1800.
[17] M.R. Morales, B.P. Barbero, T. Lopez, A. Moreno, L.E. Cadús, Fuel 88 (2009) 2122.
[18] K. Faungnawakij, N. Shimoda, T. Fukunaga, R. Kikuchi, K. Eguchi, Appl. Catal., A: Gen. 341 (2008) 139.
[19] J. Papavasiliou, G. Avgouropoulos, T. Ioannides, J. Catal. 251 (2007) 7.
[20] J. Papavasiliou, G. Avgouropoulos, T. Ioannides, Appl. Catal. B: Environ. 66 (2006) 168.
[21] J. Papavasiliou, G. Avgouropoulos, T. Ioannides, Appl. Catal. B: Environ. 88 (2009) 490.
[22] X. Du, Z. Yuan, L. Cao, C. Zhang, S. Wang, Fuel Process Technol. 89 (2008) 131.
[23] A.R.S. Rad, M.B. Khoshgouei, A.R. Rezvani, J. Mol. Catal. A: Chem. 344 (2011) 11.
[24] A.R.S. Rad, M.B. Khoshgouei, S. Rezvani, A.R. Rezvani, Fuel Process. Technol. 96 (2012) 9.
[25] Q. Huang, X. Yan, B. Li, X. Xu, Y. Chen, S. Zhu, S. Shen, J. Ind. Eng. Chem. 19 (2013) 438.
[26] X. Yan, Q. Huang, B. Li, X. Xu, Y. Chen, S. Zhu, S. Shen, J. Ind. Eng. Chem. 19 (2013) 561.
[27] M. Mansouri, H. Atashi, F.F. Tabrizi, A.A. Mirzaei, G. Mansouri, J. Ind. Eng. Chem. 19 (2013) 1177.
[28] A.C.W. Koh, L. Chen, W.K. Leong, T.P. Ang, B.F.G. Johnson, T. Khimyak, J. Lin, Int. J. Hydrogen Energy 34 (2009) 5691.
[29] M.V. Kirillova, M.F.C.G.D. Silva, A.M. Kirillov, J.J.R.F.D. Silva, A.J.L. Pombeiro, Inorg. Chim. Acta 360 (2007) 506.
[30] K. Nakamoto, Infrared and Raman Spectra of Inorganic and Coordination Compounds, Wiley-Interscience, New York, 1997.
[31] P.F. Raphel, E. Manoj, M.R.P. Kurup, Polyhedron 26 (2007) 818.
[32] W. Chen, M. Lin, T.L. Jiang, M. Chen, Int. J. Hydrogen Energy 33 (2008) 6644.